Soft Matter

Accepted Manuscript

ROYAL SOCIETY OF CHEMISTRY

www.rsc.org/softmatter

ARTICLE TYPE www. rsc.org/xxxxxx | XXXXXXXX

Striped pattern induced by delamination of drying colloidal films

F. Giorgiutti-Dauphiné,*[a] and L. Pauchard[a]

Received Xth XXXXXXXXXX 20XX, Accepted Xth XXXXXXXXX 20XX
First published on the web Xth XXXXXXXXXX 200X
DOI: 10.1039/b000000x

The drying of a dispersion of nanoparticles on a solid substrate can result in the formation of spontaneous well-ordered pattern stripes left on the substrate. The evaporation of solvent yields to large stresses in the material which usually cause crack formation and delamination from the substrate. The formation of these stripes results from a balance between the drying stress which drives the delamination crack front propagation and the cohesive properties of the material. These solid residues arise behind the crack front and can be perpendicular or parallel to the front. It is then possible to inhibit these structures by modifying the cohesive properties of the material. This self-assembly into ordered pattern can offer efficient method to produce patterning surface in a simple way.

1 Indroduction

In recent years, there has been a great deal of interest in surface patterning, since they can provide potential to achieve structures for a wide variety of applications: templates for microelectronics, optoelectronics or microfluidic devices[1–5] or arrays of magnetic nanoparticles[6]. Because of their importance in numerous applications, especially in the industry of coating, the case of planar films has motivated many works. Dispersions of nanoparticle (colloids, polymers, DNA...) self-assemble into a multitude of ordered structures upon drying. In this way, various methods have been adopted for structuring particles on a flat substrate, including controlled evaporative self-assembly. In the case of a sessile colloidal droplet on a rigid substrate, an outward flow generated inside an evaporating drop drags the particles towards the contact line. Particles are left behind and form a ring stain. When the contact line is pinned during evaporation, solute particles generally accumulate in a ring around the periphery of the drop due to the "coffee ring effect"[7,8]. The deposition of particles in ordered structures arises from the competition between the contact line pinning and the dewetting process. In some cases, the receded contact line exhibits a stick-slip motion which can induce some particular patterns exhibiting well-ordered wavelength[9,10]. The resulting morphologies mainly depend on particle concentration, particle size, interactions particle/substrate or particle/solvent. Other self-assembly patterns are observed in the geometry of dip-coating process[11]. In this case, the contact line breaks up into aggregates of nano particles to yield to the formation of aligned stripe pattern perpendicular to the contact line[12].

[a] *CNRS, UMR 7608, Lab FAST, Bat 502, Campus Univ - F-91405, Orsay, France, EU. Fax: +33 1 69 15 80 60; Tel: +33 1 69 15 80 49; E-mail: fred@fast.u-psud.fr*

Here, we report a novel yet simple method to deposit aligned stripes on substrates by the natural drying of colloidal films. During the evaporation and solidification of the films, unless they are extremely thin, large stresses develop[13]. When these stresses exceed the strength of the material, crack patterns happen whose characteristic features depend on the mechanical properties of the material[14–17]. In particular, during the delamination process, a fingering instability occurs at the delamination crack front. This results in a well-ordered solid stripes left on the substrate (figure 1c). Such stripe patterns are observed in various colloidal system, mineral, organic, and maghemite. The study deals mainly with dispersions of silica particles. From experimental results, we deduce a deposition rate for particles which can be detached from the colloidal system to be deposited on the substrate to form solid stripes. The strong influence of the cohesive strength of the gelled film is evidenced and supported by indentation testings.

2 Experimental

2.1 Materials

Five different types of particulate materials were used: concentrated aqueous dispersions of silica particles (Ludox HS-40, SM-30, TM-50 purchased from Sigma-Aldrich) and nanolatex particles (provided by Rhodia Recherche, Aubervilliers, France); HS-40 was used in most experiments. These dispersions are stable in the absence of evaporation. Values of the surface tension $\gamma_{air/water}$ of the dispersions were measured by the Wilhelmy plate method and range in $[57;67]mN.m^{-1}$. The initial viscosity η of the dispersion range in $[3;6]mPa.s$ (measurements using a rheometer Contraves LS30). For each dispersion, the weak polydispersity of the particles prevents from crystallization (polydispersity ~ 0.18). In the case of

Table 1 Main characteristics for the samples considered in the experiments. Particle diameter: $2a$, solid weight fraction ϕ_m (data given by the manufacturer Grace Davison), and solid-liquid interfacial energy γ_{SL} (measurements using indentation testing just after the crack formation).

	$2a$ (nm)	ϕ_m	γ_{SL} (J/m^2)
nanolatex PS	25	0.30	0.07
Ludox HS-40	15	0.40	
Ludox SM-30	7	0.30	
Ludox TM-50	22	0.50	0.11
Maghemite	10	0.20	

the silica sol, the stability of the dispersion is governed by the interparticle colloidal interaction (Derjaguin-Landau-Verwey-Overbeek [18,19]). In the case of the nanolatex, particles are made of polystyrene, stabilized by the presence of surfactants (SDS); since the glass transition temperature of the particles is around 100^oC, the particles are assumed to be rigid (not deformable) at room temperature. Main properties of these dispersions are reported in Table 1.

In order to study the effect of addition of polymers content in Ludox HS-40 dispersion, we use polyethylene oxyde (PEO) purchased from Sigma-Aldrich. Indeed, a high affinity for silica surfaces is known for PEO resulting in an adsorption at high coverage [20]. Molecular weight of the polymer is 600 Dalton. Polymers are dissolved in pure water at pH 9.5. This solution, with a weight concentration of polymers is noted C_p, and is used for the dilution of HS-40. As a result, the final polymer concentration in HS-40 dispersion is $C_p/4$.

2.2 Methods

A quantity of the dispersion is deposited in a shallow and circular container (wall in Altuglass, diameter $\sim$ 30mm, and height $\sim$ 5mm) and left to dry from the free surface. The substrate is a non-porous glass plate, carefully cleaned with pure water then ethanol before being dried in a heat chamber at 100°C. The contact line of the dispersion is quenched at the upper edge of the wall and remains pinned all along the drying process. At the final stage a film of approximately constant thickness is obtained in the center of the container. In this region, covering about 70% of the total surface area, the evaporation is uniform. The thickness h of the porous film is controlled by the initial volume of dispersion deposited in the container.

The mechanical properties of materials can be approached by the instantaneous response of an applied force; in this way measurements of the fracture toughness were investi-

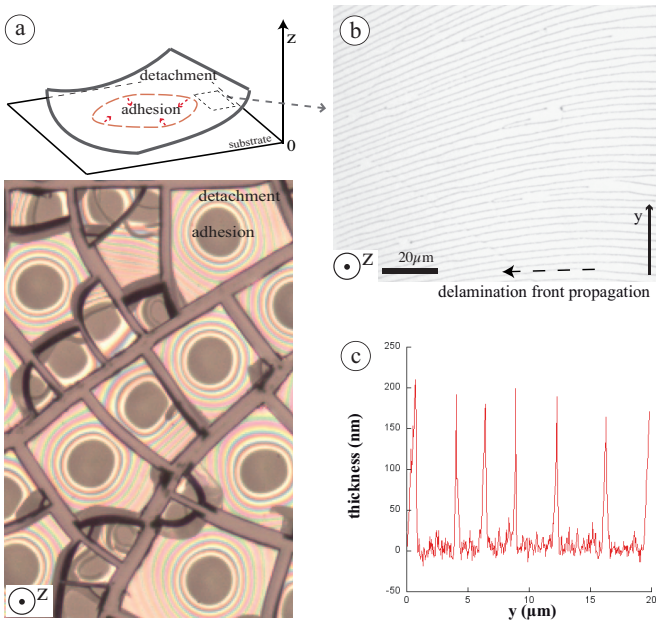

Fig. 1 (a) Partial delamination of fragments of a dry colloidal film of thickness h (image by optical microscopy in transmitted light, image height = 1.5mm). Since fragments are transparent circular optical interference fringes display an air gap between the detached film and the substrate, and encircle adhering regions (dark circular regions); the resulting curled shape is shown in the sketch. (b) Stripe pattern left on the substrate after the propagation of a delamination front in the direction of the arrow (mean spacing between lines is $\bar{\lambda} = 3\mu$m $<< h = 100\mu$m). (c) Typical cross-sectional analysis yielded the width and height of the above stripes (analysis from AFM image).

gated using indentation testing (CSM Instruments Micro Indentation testing, MHT), with a four-sided Vickers indenter tip (pyramid-shaped diamond). The indenter, initially in contact with the surface of the solid film, is driven in the material until a maximal load $F_{max} = 100$mN, with a loading speed 100mN/min. For sufficiently large indentation loads, applied to brittle materials, radial cracks emerge from the edges of the indenter (see figure 5). Same behaviours are obtained with $F_{max} = 200$mN load.

3 Results

Starting from a film of a colloidal dispersion, the solvent loss concentrates the dispersion as particles approach each other. This results in a gel phase or close-packed solid. Since the pores of the material are filled of water, further evaporation causes the liquid menisci at the top layer of the particle array to generate compressive capillary stress, and consequently tensile stress in the plane of the film, since the substrate prevents the film to shrink. When the tensile stress reaches a

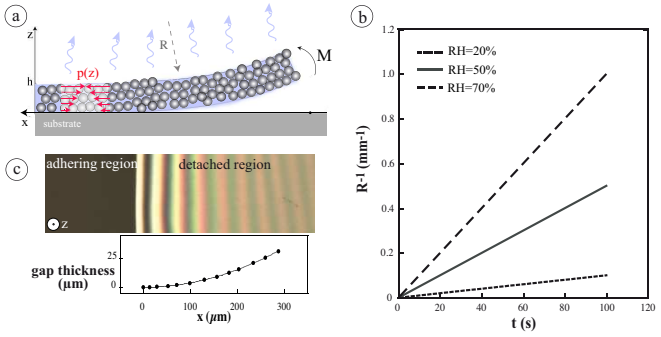

Fig. 2 (a) Sketch in side view of the delamination of a drying film induced by differential stress (liquid pressure $p(z)$ in the pores). The moment M results in a out-of-plane displacement of the film. (b) Theoretical curvature as a function of time for warping plates dried at different relative humidities RH (plates thickness is $\sim 100\mu$m). (c) Image in top view, by optical microscopy, showing interference fringes close to the delamination crack front as a result of an air gap between the transparent film and the substrate.

threshold value, successive cracks divide the solid film into sided domains resulting in the typical pattern shown in figure 1a. Since the film still dries from only one side, the porous network is compressed more on the drying face: a moment M results in a out-of-plane deformation of the film (figure 2a). Consequently the fragment becomes concave toward the drying side, with a characteristic curvature R^{-1} that is time-dependent. Indeed, the curvature of a warping plate increases rapidly with the evaporation rate V_E as predicted by a simple scaling law for the warping of a plate[21,22]: $R^{-1} \sim \frac{V_E}{h^2}t$ (figure 2b). This deformation drives the propagation of the delamination crack front that separates the adhering region from the detached one (figure 2c). During the delamination process the crack front usually destabilizes into a finger-like front (figure 3). This leaves periodic stripes made of particles on the substrate; stripes are normal to the delamination crack front, as shown in figure 1b.

Analysis from Atomic Force Microscopy reveals the typical dimensions of these stripes (figure 1c): mean width $= 0.8\mu$m, mean height $= 175$nm which is lower than the film thickness h, and the characteristic distance between adjacent stripes $\lambda = 3\mu$m. A consequence of the deposition of particles on the substrate is the formation of negative dimpled stripes in backside of delaminated fragments (figure 3). Note that the size of the striped pattern is reproducible for a given system. The height of the lines of deposited particles can be roughly estimated using the following considerations. In general a crack advances only if the stress intensity factor K reaches the fracture toughness K_c that represents the material resistance to fracture. Assuming the material is linear elastic, $K \sim \sigma\sqrt{H}$, where σ is the mechanical stress in the film and H is a length scale of the opening crack, and $K_c = \sqrt{\Gamma E}$, where E is the

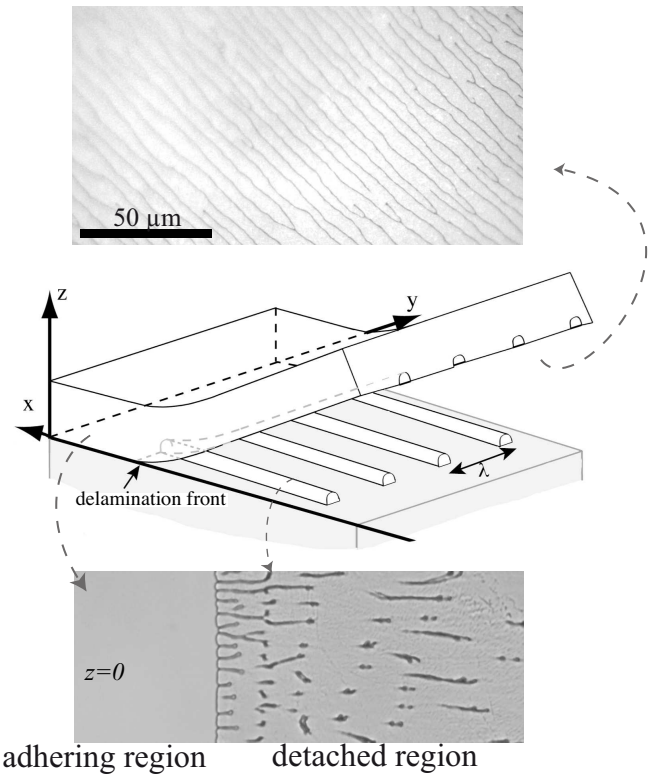

Fig. 3 Sketch showing the formation of stripes left on the substrate behind the delamination crack front: the delamination front propagates along the x-axis. Above: backside of a delaminated fragment showing the negative dimpled stripes. Below: image of the stripes formation behind the destabilizing crack front.

Young's modulus of the film and Γ is equal to the work used to create the new crack surfaces, work of adhesion in the case of an interfacial crack (assuming adhesion is due to the meniscus around each colloidal particle, $\Gamma \sim 10^{-2} J.m^{-2}$). The maximum value of the interfacial crack opening, H_m, corresponds to the maximum value of the stress, σ_m, in the film, close to the capillary pressure, P_{cap}, as: $H_m \sim \frac{\Gamma E}{(-P_{cap})^2} = \frac{10^{-2}.10^9}{(-10^7)^2} \sim 1\mu m$. H_m gives an order of magnitude of the height of the lines of deposited particles and is in agreement the height measured with AFM (image in Figure 1(c)).

The well ordered pattern results from the well-known hydrodynamic instability, i.e., the Saffman-Taylor instability for viscous fluids[23]. This instability usually occurs to the interface between two viscous and immiscible fluids when the less viscous one invades the more viscous one. In our case, the interface is moving with v_f, the delamination crack front velocity, and separates two immiscible fluids, air and the concentrated dispersion. Thus, the wavelength λ of the finger-like front which is the most amplified can be expressed as: $\lambda \sim \xi\sqrt{\frac{\gamma_{air/water}}{\eta.v_f}}$, where ξ is a length scale where the debond-

ing occurs[24]. The range of action of the debonding process is the meniscus around each colloidal particle, so we estimate ξ equal to a fraction of the particle size. It comes $\lambda \sim 10^{-9}\sqrt{\frac{70\times10^{-3}}{10^{-3}.3\times10^{-6}}} \sim 4\mu$m, in agreement with the length scale measured in our systems. The expression for λ proposed is proportional to the particles size and inversely proportional to the front velocity. As the front velocity increases with the particles size, a change in the particles size implies no significant variations for λ. Thus, the measurements of λ are the same in images of Figure 5: $7\pm1\mu$m (Fig. 5b) $6\pm1\mu$m (Fig. 5c) $8\pm1\mu$m (Fig. 5d, for stripes perpendicular to the front). Nevertheless, the particles size plays a significant role on the front velocity, and on the rigidity of the material, as evidenced by results using the indentation testing. This last point could be quantified by the following expression ([25]):

$$E \infty \phi^4 (\frac{E_0^2 \gamma}{a})^{1/3}$$

with E_0 and E, the elastic moduli of respectively a single particle and of the system. γ is the surface energy of a particle and a the radius of a particle. Thus with small particles (SM-30), the system is more rigid, and no stripe pattern are observed because the cohesion force is higher than the capillary pressure. One can note that the viscosity of the solvent can be modified using a cosolvent such as glycerol exhibiting high miscibility with water. However addition of a concentration greater than 10% to a dispersion results in a crack free coating. This concentration range is not sufficient to affect significantly the wavelength of finger-like front[26]. The formation of the solid stripes requires first the destabilisation of the delaminated crack front to form a finger-like front, then particles have to be expelled from the cohesive gel to form settling aggregates on the substrate. Theses aggregates account for nucleation centers to collect further particles as the delamination crack front advances to finally form the residues (inset in figure 4b). Strong forces are required to expel particles from the cohesive gel (figure 2c). This is achieved in the small opening angle between the film and the substrate, close to the delamination crack front. Indeed, in this confined area, an interface between the liquid meniscus and air is subjected to large capillary pressure due to the large curvature of the interface. This large capillary pressure possibly overcomes the cohesion of the material, and consequently restructures the colloidal packing.

As a result, a fraction ϕ_d of particles in the water-supported film can be detached from the colloidal packing and then deposits onto the substrate. The deposition process results from the competition between the speed of the delamination crack front v_f and the particles deposition rate v_d, similarly to the competition between a liquid contact line velocity and the particle deposition rate studied by Yang et al.[27]. The deposition rate v_d depends mainly on the volume fraction of particles ϕ_d

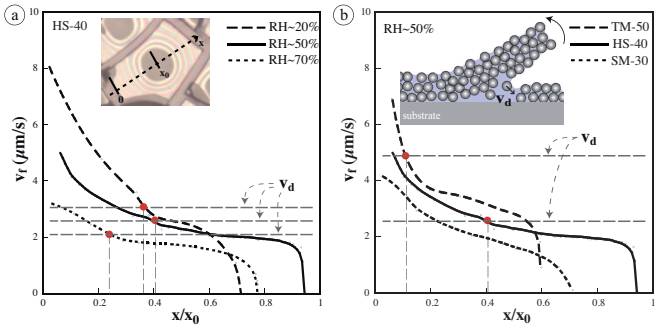

Fig. 4 Speed v_f of the delamination crack front along the x-axis ($x=0$ corresponds to the fragments limit, and $x=x_0$ is located at the center of the circular adhering region) (a) for silica films (HS-40) dried at different relative humidity RH, and (b) for different silica films (TM-50, HS-40, SM-30) dried at $RH \sim 50\%$. Reduced speed causes the development of fingering instabilities, indicated by the red dot, resulting in the formation of the stripes pattern on the substrate. The deposition process can be approached by considering a mismatch between the speed of the crack front and a characteristic speed v_d of particles deposition (inset).

available to deposit onto the substrate, and on the evaporation rate as: $v_d \propto \phi_d V_E$, for $\phi_d << 1$, where the proportionality coefficient depends on the particle-particle and particle-substrate interaction[28]. Assuming the quantity ϕ_d constant during the delamination process, the deposition rate v_d is kept constant, for given drying conditions. Thus, one can defined a criterion for the formation of the solid stripes: for $v_f > v_d$, particles have not enough time to deposit onto the substrate, no residue are left on the substrate, while the condition $v_f < v_d$ states for the stripes to form. The experimental results reported on figure 4 provide estimation for v_d. The data in Figure 4-a, concern measurements of the speed of the delamination crack front for different drying conditions and for one system (silica films HS-40). In general, when the debond length exceeds several times the film thickness, the delamination crack front velocity decreases until a roughly constant value (a typical value of the velocity v_f is then a few μm/s, greater than the evaporation rate $= 5\times10^{-8}$m/s), till fingering instability occurs. The red dots in the graph, correspond to the appearance of the first residue. The corresponding velocity v_f represents then the critical velocity by when the particles are deposited on the substrate, that is v_d. The experiments reveal weak influence of the relative humidity on the values of v_d (roughly 1 μm/s for RH ranges between 20 and 70 % in figure 4a). This can be understood as the wet debond front is a very confined area where evaporation is very low. Values v_d deduced from figure 4a range between 2 and 5μm/s, which is in agreement with calculated deposition speeds for diluted particle suspensions close to 5% in reference[28].

We report in figure 4b the formation of stripe pattern for dif-

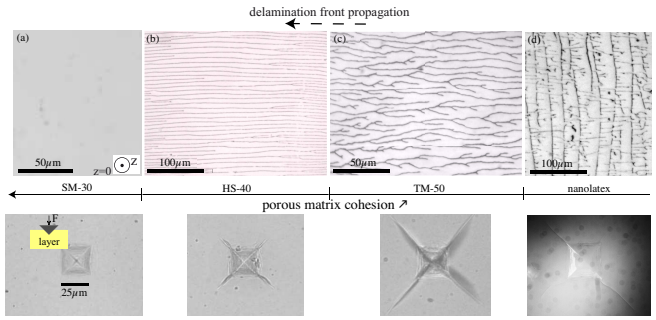

Fig. 5 Typical patterns at the surface of the substrate after delamination process of different films: (a) deposition-free (SM-30), (b) stripe pattern (HS-40), (c) fork (TM-50), (d) stripes and ring patterns (nanolatex). Below: prints of indent for the different films: short or long radial cracks can nucleate from the indent, and are characteristic of the fracture toughness of the material.

ferent colloidal systems, keeping the drying conditions constant; results are reported in table 1 for colloidal gels of silica particles (SM-30, HS-40 and TM-50) and organic particles (nanolatex). In particular particle size and particle charge of the colloidal film affect the occurrence of the fingering instability, also the stripe pattern. The deposition rate v_d is higher for TM-50 than for HS-40, whereas for silica particle SM-30, no stripe patterns are formed. This results highlight the role of the cohesion of the system on the formation of the stripes. v_d depends on the size of the particles as it stands for the velocity for a particle to move on a distance close to its diameter. Moreover, for too smallest particles (silica particle SM-30), the capillary forces cannot overcome the cohesive strength of the material. Thus the resulting volume fraction of particles ϕ_d available to deposit onto the substrate is larger for TM-50 than for HS-40 and close to 0 for SM-30. For gels made of nanolatex particles, the stripe pattern is more complex due to two modes of propagation of the delamination crack front: fingering instability resulting in stripes perpendicular to the delamination crack front, and stick-slip motion leading to stripes parallel to the front (figure 5d). These observations strongly suggest that the formation of the stripe patterns on a substrate depends on the physicochemical and mechanical properties of the delaminated gel.

Stripe patterns are strongly dependent on the fraction of particles available to deposit onto the substrate, and by the way, on the cohesive strength of the material. Indeed, due to the small opening angle between the film and the substrate, particles can be detached form the gel if the cohesive strength of the gel is low. On the contrary, we expect no stripe pattern on the substrate for films exhibiting high cohesive strength. A simple way to compare the cohesive strength of dried films is to observe the ability of materials to propagate crack or resist crack propagation by indentation testing (see Experimental section). For sufficiently large indentation loads, radial cracks emerge from the edges of a Vickers indenter (see figure 5). Therefore, different dried films are compared in figure 5. Except for dried films of SM-30, indentation load leads to radial cracks, and stripe pattern due to delamination process: consequently films of SM-30 reveal a higher cohesive strength than others studied films. For dried films exhibiting a high cohesive strength, no radial cracks due to indentation load (SM-30)and no stripe pattern due to delamination process are observed as it is the case for films with lower cohesive strength (HS-40, TM-50, nanolatex). Note that, from experimental results, the higher cohesive strength is typical of gel made of small particles size. It is then possible to prevent the formation of the well-ordered stripe pattern observed in HS-40 films, for example, by modifying the cohesive properties of the material. A way to do that is to increase the cohesive strength of the gel, by adding polymers; the internal bonding between particles is modified by adsorbing polymer chains (PEO) at particle surface [20]. We have observed that the surface of the substrate is free of stripes after the film delamination process. This result confirms that a low cohesive strength is necessary to form stripe pattern during the delamination process.

4 Conclusion

During the drying of a colloidal film of nanoparticles usually exhibits mechanical instabilities resulting in cracks formation and delamination process. The delamination crack front can destabilizes into a finger-like front. This leaves periodic solid stripes, perpendicular to the interfacial crack front. The potential application of this phenomenon could be the formation of patterning substrates providing the deposition area is important comparing to the total surface of a fragment. We found for our experiments, a typical deposition area of stripe patterns of about $1/3$ of the total surface of a fragment. Measurements by image processing show that residues cover 15% of the surface of the substrate. Capillary forces occuring in the confined area between the substrate and the film close to the delaminated front can overcome the cohesive strengths provided there are low enough. Experimental results evidence the role of the cohesive strength of different materials using indentation testing. In particular the modification (decrease) of the cohesive strength of a film by adsorbing polymer chains to colloidal particle surface inhibits the stripe patterns.

References

1 N. Tas, T. Sonnenberg, H. Jansen, R. Legtenberg and M. Elwenspoek, *J. Micromech. and Microeng.*, 1996, **6(4)**, 385 – 397.
2 C. Mastrangelo, *Tribology Letters*, 1997, **3**, 223 – 238.
3 C. Hui, A. Jagota, Y. Lin and E. Kramer, *Langmuir*, 2002, **18(4)**, 1394 – 1407.
4 C. S. Davis and A. J. Crosby, *Soft Matter*, 2011, **7**, 5373–5381.

5 Y. Ebata, A. B. Croll and A. J. Crosby, *Soft Matter*, 2012, **8**, 9086–9091.
6 J. Shi, S. Gider, K. Babcock and D. D. Awschalom, *Science*, 1996, **271**, 937 – 941.
7 R. D. Deegan, O. Bakajin, T. F. Dupont, G. Huber, S. R. Nagel and T. A. Witten, *Nature*, 1997, **389**, 827–829.
8 R. Deegan, *Phys Rev E*, 2000, **61**, 475.
9 E. Adachi, A. S. Dimitrov and K. Nagayama, *Langmuir*, 1995, **11**, 1057–1060.
10 S. Maheshwari, L. Zhang, Y. Zhu and H.-C. Chang, *Phys. Rev. Lett.*, 2008, **100**, 044503.
11 J. Huang, F. Kim, A. Tao, S. Connor and P. Yang, *Nature Materials*, 2005, **4**, 896 – 900.
12 W. Han, B. Li and Z. Lin, *ACS Nano*, 2013, **7**, 6079–6085.
13 P. Xu, A. S. Mujumdar and B. Yu, *Drying Technology: An International Journal*, 2009, **27**, 636–652.
14 J. W. Hutchinson and Z. Suo, *Adv. Appl. Mechs.*, 1992, **29**, 63.
15 A. Groisman and E. Kaplan, *Europhys. Lett.*, 1994, **25**, 415–420.
16 L. Pauchard, *Europhys. Lett.*, 2006, **74**, 188 – 1891.
17 V. Lazarus and L. Pauchard, *Soft Matter*, 2011, **7**, 2552–2559.
18 B. Derjaguin and L. Landau, *Acta Physicochim URSS*, 1941, **14**, 633.
19 E. J. Verwey and J. T. G. Overbeek, *Theory of Stability of Lyophilic Colloids*, Elsevier, Amsterdam, 1948.
20 K. Wong, P. Lixon, F. Lafuma, P. Lindner, O. A. Charriol and B. Cabane, *Journal of Colloid and Interface Science*, 1992, **153**, 55 – 72.
21 C. J. Brinker and G. W. Scherer, *Sol-Gel Science: The Physics and Chemistry of Sol-Gel Processing*, Elsevier Science, 1990.
22 F. Giorgiutti-Dauphiné and L. Pauchard, *Eur. Phys. J. E*, 2014, **XXX**, year.
23 P. Saffman and G. Taylor, *Proceedings of the Royal Society A*, 1958, **245**, 312 – 329.
24 R. J. Fields and M. F. Ashby, *Philosophical Magazine*, 1976, **33**, 33 – 48.
25 K. Kendall, N. M. Alford and J. D. Birchall, *Proc. R. Soc. Lond. A*, 1987, **412**, 269.
26 F. Boulogne, L. Pauchard and F. Giorgiutti-Dauphiné, *Soft Matter*, 2012, **8**, 8505.
27 X. Yang, C. Y. Li and Y. Sun, *Soft Matter*, 2014, **10**, 4458–4463.
28 B. Prevo and O. Velev, *Langmuir*, 2004, **20**, 2099–2107.

5 Acknowledgment

We thank Patrick Guenoun (LIONS-CEA), and Mokhtar Adda-Bedia (LPS-ENS) for useful discussions, Alban Aubertin, Lionel Auffray, Christian Borget, and Rafaël Pidoux (FAST-University Paris Sud) for engineering and technical support.